

## Original article

# Construction of PAN-based activated carbon nanofibers for hydrogen storage under ambient pressure

Junwei Yu<sup>1,2,4</sup>, Tianhao Lin<sup>3</sup>, Jialin Li<sup>2</sup>, Wanqin Zhang<sup>2</sup>, Wenzhe Bao<sup>2</sup>, Bo Zhu<sup>2</sup>\*

<sup>1</sup>Center for Optics Research and Engineering, Shandong University, Jinan 250100, P. R. China

<sup>2</sup>Key Laboratory of Liquid-Solid Structural Evolution and Processing of Materials of Ministry of Education, Shandong University, Jinan 250061, P. R. China

<sup>3</sup>College of Chemical and Pharmaceutical Engineering, Shandong First Medical University, Taian 271016, P. R. China

<sup>4</sup>Guangdong Provincial Key Laboratory of Advanced Energy Storage Materials, South China University of Technology, Guangzhou 510640, P. R. China

### Keywords:

Activated carbon nanofibers  
polyacrylonitrile  
atmospheric hydrogen storage  
adsorption isotherm model

### Cited as:

Yu, J., Lin, T., Li, J., Zhang, W., Bao, W., Zhu, B. Construction of PAN-based activated carbon nanofibers for hydrogen storage under ambient pressure. *Capillarity*, 2023, 6(3): 49-56.  
<https://doi.org/10.46690/capi.2023.03.02>

### Abstract:

Adsorption agents are an important class of solid hydrogen storage materials. Attributed to their high specific surface area and adjustable nanopore structure, activated carbon nanofibers have attracted extensive attention in the application of solid hydrogen storage. The research in this field mostly focuses on applications with a hydrogen pressure condition of 30 to 300 bar, while there have been few systematic studies on the hydrogen storage performance of these materials under ambient pressure. In this study, polyacrylonitrile-based activated carbon nanofibers were constructed by electrospinning technology and ultrasonic-assisted activation technology for the application of atmospheric hydrogen storage. Their nanopore structure was revealed to be mainly composed of micropores, and the relative contents of micropore volume and ultramicropore volume were 77.92% to 88.3% and 22.34% to 24.68%, respectively. Attributed to the synergy of rich microporous structure and surface chemical structure, the atmospheric hydrogen storage density of activated carbon nanofibers could reach 2.64 wt% at 77 K and 1 bar. After the optimization analysis of adsorption isotherm models, the Multisite-Langmuir model was found as more suitable for accurately describing the atmospheric hydrogen adsorption process of activated carbon nanofibers.

## 1. Introduction

Hydrogen is an excellent secondary energy carrier with the characteristics of environmental friendliness, vast resources, high calorific value, exceptional combustion performance, and no instability disadvantage limited by time and region, such as solar energy, wind energy, etc. (Schoedel et al., 2016; Chen et al., 2020; Sun et al., 2020). Due to the active chemical properties of hydrogen, safe and efficient hydrogen storage technology is the main bottleneck for the application and promotion of hydrogen energy, with the most difficult technical obstacles to overcome being hydrogen storage density and

storage cost (Wang et al., 2020; Wu et al., 2020; Mahdi et al., 2021). Currently, high-pressure and liquefied hydrogen storage are the most mature hydrogen storage technologies, yet they both have the insurmountable disadvantages of high cost and low safety (Li et al., 2021; Jaramillo et al., 2021; Nguyen et al., 2022).

Solid-state hydrogen storage technology with high safety, high hydrogen storage density and low cost is considered to be the future development direction. Under the action of nanopore structure, adsorption-type porous materials can achieve high adsorption potential energy for most gas adsorbates, thus realizing the efficient adsorption and storage of specific gases

(Liu et al., 2022; Wang et al., 2023). In addition, the research on adsorptive hydrogen storage materials mostly focuses on the hydrogen pressure condition of 30-300 bar, while there have been few systematic researches evaluating the conditions of ambient pressure (Blankenship et al., 2017; Allendorf et al., 2018; Balahmar and Mokaya, 2019). Similar to normal temperature superconducting technology, atmospheric hydrogen storage can eliminate the hidden safety hazards brought about by high-pressure containers and greatly reduce the cost of hydrogen storage. It has been highlighted that the realization of solid-state hydrogen storage under environmental conditions will greatly promote the large-scale application of hydrogen energy (Lim et al., 2012; Yuan et al., 2019).

Activated carbon nanofibers, with high specific surface area and adjustable nanopore structure, have attracted extensive attention from researchers in the field of adsorption and purification, and their solid hydrogen storage applications also show excellent application prospects (Fan et al., 2011; Waisi et al., 2019; Zakaria et al., 2021; Real et al., 2022). Kim et al. (2011) synthesized uniform nanoporous carbon nanofibers with Pd nanoparticles using water vapor as a nanoscale pore former, and the prepared nanofibers exhibited a large specific surface area of 1,121 m<sup>2</sup>/g and a hydrogen adsorption capacity of 2.3 wt% at 77 K, 1 bar and 0.82 wt% at 298 K, 1 bar. Yadav et al. (2017) prepared Ni-containing microporous and graphitic carbon nanofiber (CNF)-based adsorbent, and the hydrogen storage density could reach 0.75 wt% at 298 K and 50 bar. Similar to most adsorptive hydrogen storage materials, investigations on the hydrogen storage performance of this material were mostly conducted at the saturated adsorption pressure of 30 to 300 bar or extremely low temperature conditions such as liquid nitrogen. In this work, based on electrospinning technology and sonication-assisted activation technology, activated carbon nanofibers with high specific surface area and rich surface groups were prepared using polyacrylonitrile as a precursor. Under the synergy of physisorption and chemisorption, the prepared activated carbon nanofibers exhibited excellent hydrogen storage performance under ambient pressure. Our results promote the study of unsaturated adsorption hydrogen storage by adsorptive materials under environmental conditions.

## 2. Experimental section

### 2.1 Synthesis of PAN-based activated carbon nanofibers

Polyacrylonitrile (PAN) solution with a mass fraction of 10 wt% was prepared by using PAN (molecular weight 220,000) as solute and dimethyl sulfoxide as solvent, then PAN-based nanofibers (labeled as CNF) were prepared through electrospinning technology and pre-oxidized at 533 K. Preoxidized carbon nanofiber (labeled as PO-CNF) was activated by an ultrasound-assisted process, which mainly included three steps of ultrasonic-assisted impregnation, high-temperature activation and water washing. The first step was to impregnate the pre-oxidized carbon nanofibers with phosphoric acid solution as a chemical activator, with a mass fraction of 15 wt% under 333 K for 360 mins. We placed the nanofiber samples impreg-

nated with activator into a tubular furnace for high-temperature activation under nitrogen or carbon dioxide atmospheres, with an activation temperature of 1,123 K and activation time of 30 min. The activated samples were fully washed in deionized water to finally obtain activated carbon nanofibers (ACNFs). ACNFs prepared by activation in nitrogen and carbon dioxide atmosphere were respectively named as ACNF-1 and ACNF-2.

### 2.2 Characterization

SU-70 thermal field emission scanning electron microscope (JEOL company, Japan) was adopted to observe microscopic morphology with an accelerating voltage of 10 kV. The crystal structure was determined by X-ray powder diffraction (XRD) on a Rigaku D/max-RC X-ray diffractometer operated by Cu K $\alpha$  radiation ( $\lambda = 1.54 \text{ \AA}$ ) at a scan speed of 5° min<sup>-1</sup>. Raman spectra were measured by a Renishaw inVia micro-confocal Raman spectrometer with laser excitation wavelength of 632.8 nm and Raman shift ranged between 1,000 to 2,000 cm<sup>-1</sup>. IR analysis was performed by TENSOR37 infrared spectroscopy (Bruker Company) with a scanning range of 500-4,000 cm<sup>-1</sup>. The nitrogen adsorption isotherm and hydrogen adsorption isotherm were determined by Autosorb-iQ3 equipment (Quantachrome, USA) in the liquid nitrogen environment, and the pretreatment temperature was set at 473 K for 720 min.

## 3. Results and discussion

### 3.1 Microscopic morphology

As shown in Fig. 1(a), the prepared CNF fiber has a large surface roughness and no obvious groove structure, and its diameter is about 985 nm. After pre-oxidation treatment, the fiber diameter of PO-CNF decreases to 683 nm (Fig. 1(b)), and its surface roughness continues to increase with the formation of a macroporous structure. Both the fiber diameter change and the formation of macropore structure are caused by the shrinkage of polyacrylonitrile molecules and the volatilization of residual solvents during the pre-oxidation process. The micromorphology of activated carbon nanofibers ACNF-1 and ACNF-2 are shown in Figs. 1(c) and 1(d), respectively. After activation, ACNF-1 and ACNF-2 still maintain a uniform fibrous structure, and the surface roughness is relatively flat. The surface roughness of ACNF-2 fiber activated in carbon dioxide atmosphere is better than that of ACNF-1. It is worth noting that the fusion bonding phenomenon between PAN nanofibers occurs in carbon nanofibers after activation, which may have a negative impact on the formation of nanopore structure and hydrogen storage performance.

### 3.2 Crystal structure

The XRD pattern of CNF is shown in Fig. 2, which apparently contains a diffraction peak near 17° representing (100) crystal plane structure of PAN crystal cell and a dispersion peak near 27° that corresponds to the amorphous structure of PAN molecular chain (Liu et al., 2012; Díez et al., 2017; Yu et al., 2023). For the crystal structure of CNF, the calculated grain size  $L_c = 3.07 \text{ nm}$  and the crystallinity  $C$  is 28.39% (Haddad et al., 2018; Sahoo et al., 2021). After pre-oxidation

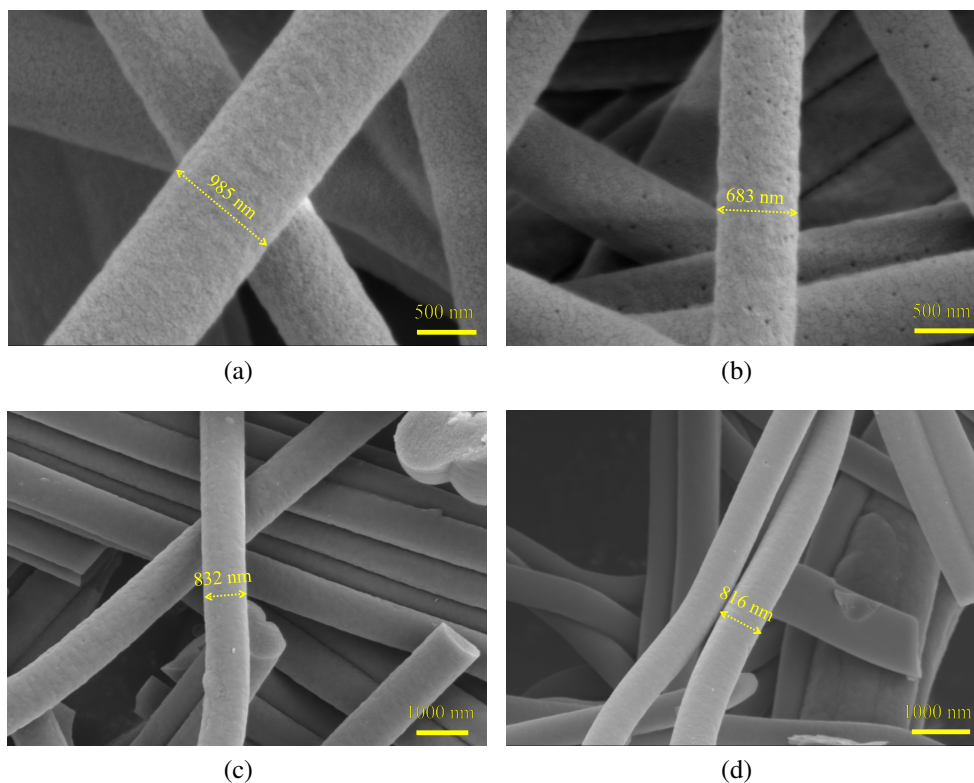


**Fig. 1.** Microscopic morphology. (a) CNF, (b) PO-CNF, (c) ACNF-1 and (d) ACNF-2.

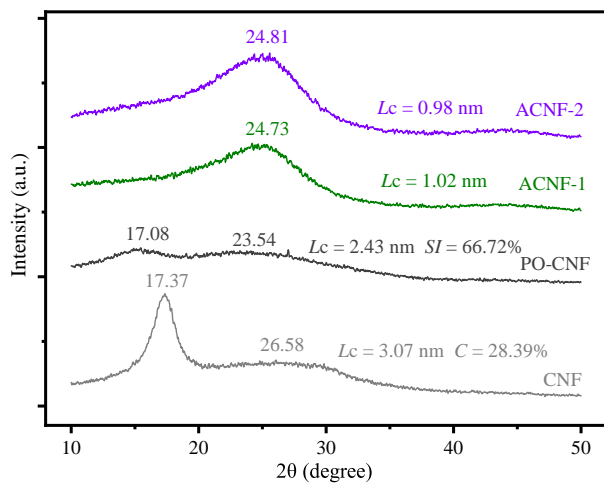


**Fig. 2.** XRD spectra of PAN-NF, PO-CNF and ACNF.

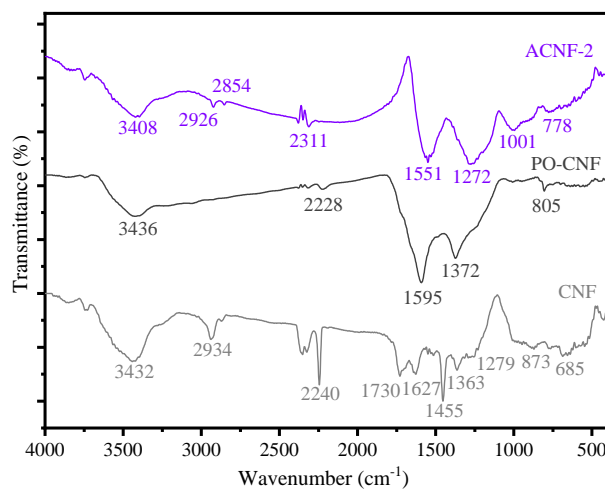


**Fig. 3.** FT-IR spectra of PAN-NF, PO-CNF and ACNF-2.

treatment, the diffraction peak intensity of (100) crystal plane near  $17^\circ$  decreases, and the dispersion peak of amorphous phase shifts to  $23.5^\circ$ . For the crystal structure of PO-CNF, the calculated grain size  $L_c = 2.43$  nm and the pre-oxidation index  $SI = 66.72\%$ , indicating that the crystal microstructure of PAN-PONF changes during the pre-oxidation process, that is, the linear macromolecular chain of PAN transforms into a ring structure. As the pre-oxidation temperature rises to above 508 K, the original quasicrystal system is damaged by heat and gradually becomes a relatively stable trapezoidal polymer structure, eventually leading to the phenomenon of grain size reduction and crystallinity reduction during the pre-oxidation

process (Madrakian et al., 2018; Zhang et al., 2021).

After high-temperature activation at 1,123 K, the XRD spectra of ACNF-1 and ACNF-2 show a main dispersion peak near  $24.8^\circ$  caused by the (002) crystal plane of graphite-like microcrystalline, while the (100) crystal plane diffraction peak of PAN crystal cell near  $17^\circ$  completely disappears. The grain sizes  $L_c$  of ACNF-1 and ACNF-2 are 1.02 and 0.98 nm, respectively. In the process of high-temperature activation, the trapezoidal macromolecules are further denitrogenated and cross-linked to form a network of macromolecular carbon layers and rearranged into a graphite-like microcrystalline carbon structure. At the same time, accompanied by oxidation

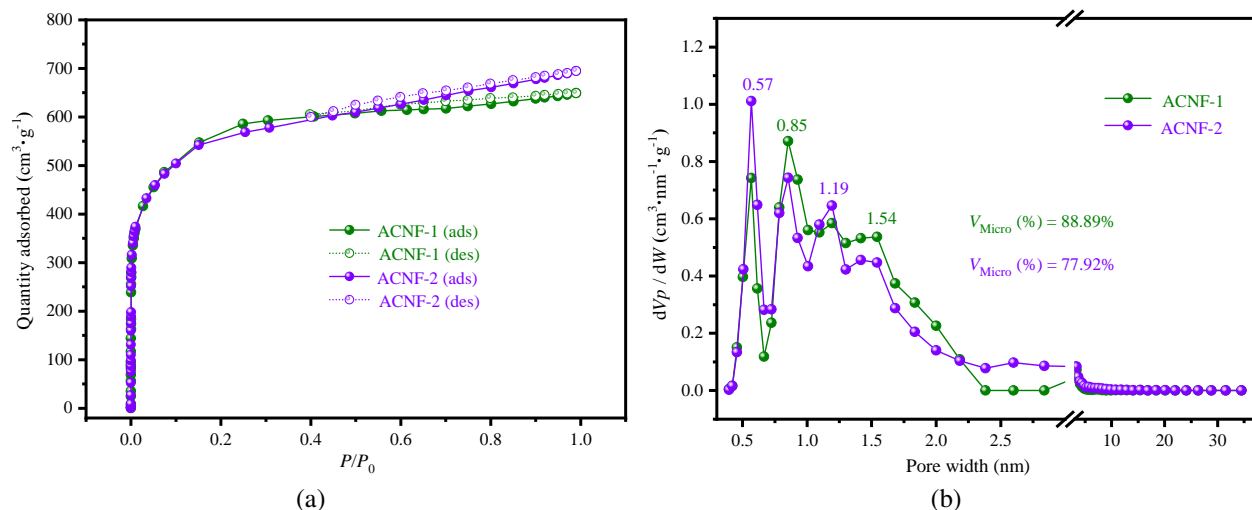


**Fig. 4.** Nanopore structures of ACNF-1 and ACNF-2.

**Table 1.** Langmuir model and empirical equations for monolayer sorption.

Sample	ACNF-1	ACNF-2
$S_{BET}$ (m <sup>2</sup> /g)	1,994.03	2,007.66
$V_{Tot}$ (cm <sup>3</sup> /g)	0.94	1.01
$V_{Micro}$ (cm <sup>3</sup> /g)	0.83 (88.30%)	0.78 (77.92%)
$V_{Ultra}$ (cm <sup>3</sup> /g)	0.21 (22.34%)	0.25 (24.68%)
$V_{Meso}$ (cm <sup>3</sup> /g)	0.11 (11.70%)	0.22 (22.08%)
Average aperture (nm)	2.02	2.14

and erosion, the graphite-like microcrystalline porous carbon structure develops small grains and micropores (Smith et al., 2014; Xu et al., 2018; Yu et al., 2021).

### 3.3 Surface chemical structure

CNF, PO-CNF and ACNF were subjected to FT-IR analysis to further determine the evolution of surface chemical structure during the preparation of activated carbon nanofibers. The main infrared characteristic peaks of PAN-NF include 3,432 cm<sup>-1</sup> ( $\nu_{O-H}$  or  $\nu_{N-H}$ ), 2,934 cm<sup>-1</sup> ( $\nu_{C-H}$ ), 2,240 cm<sup>-1</sup> ( $\nu_{C\equiv N}$ ), 1,730 cm<sup>-1</sup> ( $\nu_{C=O}$ ), 1,627 cm<sup>-1</sup> ( $\nu_{COO}^{as}$ ), 1,455 cm<sup>-1</sup> ( $\nu_{COO}^s$ ), and 1,363 cm<sup>-1</sup> ( $\delta_{C-H}$ ). (Kizildag et al., 2016; Ismar and Sarac, 2017). It can be seen that the surface groups of prepared CNF mainly include nitrile group, carboxyl group, carboxyl ion, and ammonium ion, and the hydrolysis reaction of nitrile group occurred on the fiber surface. The infrared characteristic peaks of PAN-NF mainly include 3,436 cm<sup>-1</sup> ( $\nu_{O-H}$  or  $\nu_{N-H}$ ), 1595 cm<sup>-1</sup> ( $\nu_{C=N}$  or  $\nu_{C=O}$ ) and 1,372 cm<sup>-1</sup> ( $\nu_{C-O}$ ). After the pre-oxidation treatment, the surface groups of PO-CNF fibers are mainly hydroxyl, carboxyl, C=N and residual nitrile groups. The infrared characteristic peaks of ACNF-2 are mainly at 3,408 cm<sup>-1</sup> ( $\nu_{O-H}$  or  $\nu_{N-H}$ ), 2,926 cm<sup>-1</sup> ( $\nu_{C-H}$ ), 1,551 cm<sup>-1</sup> ( $\nu_{C=N}$  or  $\nu_{C=O}$ ), 1,272 cm<sup>-1</sup> ( $\nu_{C=O}$ ), 1,001 cm<sup>-1</sup> ( $\delta_{C-H}$  in pyridine structure), and 778

cm<sup>-1</sup> ( $\gamma_{C-H}$  in pyridine structure) (Tan et al., 2020; Ying et al., 2020). These data indicate that the surface groups of activated carbon nanofibers are essentially hydroxyl, carboxyl and pyridine. Rich functional groups will effectively enhance the hydrogen adsorption potential energy on the fiber surface, and the adsorption and hydrogen storage process of ACNF will be carried out under the coordination of physisorption and chemisorption. The positive effect of oxygen functional groups is expected to significantly improve the enhancement of hydrogen storage performance at low pressure, where the interaction between hydrogen and the surface is more important than that at higher pressure where hydrogen uptake is more likely to occur via space filling mechanisms (Blankenship et al., 2017; Balahmar and Mokaya, 2019).

### 3.4 Nanopore structure of ACNF

The nitrogen adsorption test results are shown in Fig. 4(a), where both isotherm curves of ACNF-1 and ACNF-2 belong to the type I (Langmuir) adsorption isotherm representing microporous materials, and the adsorption platform appears on the isotherm when the adsorption amount reaches about 600 cm<sup>3</sup>/g (Qiao et al., 2020; Ahn et al., 2021). The adsorption equilibrium is rapidly reached in the low pressure region ( $P = 0$  to 0.15 bar), then multilayer adsorption occurs and the adsorption amount presents a slowly increasing state of uniformity, indicating that the nanopore structure of ACNF-1 and ACNF-2 mainly includes micropores.

The Brunauer, Emmett and Teller (BET) equation and density functional theory (DFT) model calculation results in Table 1 show that the specific surface area, total pore volume, micropore volume, ultramicropore volume, and mesoporous volume of ACNF-1 are 1,994.03 m<sup>2</sup>/g, 0.94, 0.83, 0.21, and 0.11 cm<sup>3</sup>/g, respectively. Under the joint action of phosphoric acid and carbon dioxide activator, the specific surface area, total pore volume, extremely microporous volume, and mesoporous volume of ACNF-2 are increased by 0.68%, 7.45%, 19.05% and 100% respectively, while the microporous volume

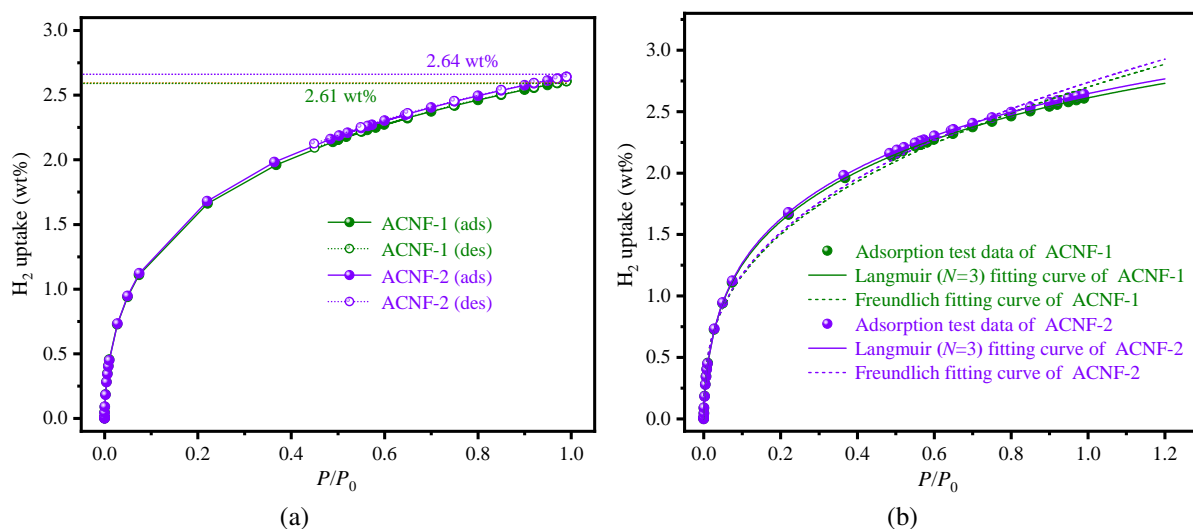


**Fig. 5.** Analysis of hydrogen adsorption/desorption process at 77 K and 1 bar.

**Table 2.** Isothermal adsorption model parameters.

Models	Parameters	ACNF-1	ACNF-2
Multisite-Langmuir $Q = \frac{\sum_{i=1}^3 Q_{ei} K_{Li} P}{1 + \sum_{i=1}^3 K_{Li} P}$	$Q_{e1}$	2.3908	2.4104
	$Q_{e2}$	1.1134	1.1538
	$Q_{e3}$	0.3399	0.3395
	$K_{L1}$	1.0463	1.0272
	$K_{L2}$	16.6972	16.1459
	$K_{L3}$	350.1749	336.5360
	$R^2$	1	1
Freundlich $Q = K_F P^{1/n}$	$K_F$	2.7002	2.7381
	$1/n$	0.3646	0.3668
	$R^2$	0.9967	0.9965

is decreased by 6.02%. These data demonstrate that the introduction of carbon dioxide activator has a weaker influence on the surface area in the ultrasound-assisted phosphoric acid activation process, which is more conducive to the formation of micropores and mesopores. To further explore the pore size distribution of activated carbon nanofibers, the pore size distribution of ACNF-1 and ACNF-2 is analyzed by the DFT method. The pore size distributions of ACNF-1 and ACNF-2 are roughly the same, with micropores mainly concentrated at 0.57, 0.85, 1.19 and 1.54 nm. The difference is that the maximum pore volumes of ACNF-1 and ACNF-2 appear at 0.85 and 0.57 nm, respectively, and the pore volume at 0.57 and 2.2 to 3 nm of ACNF-2 is larger than that of ACNF-1, which is consistent with the change trends of micropore volume and mesopore volume.

### 3.5 Atmospheric hydrogen storage performance of ACNF

As shown in Fig. 5(a), the hydrogen adsorption isotherms of ACNF-1 and ACNF-2 belong to the type I adsorption

isotherm generated by microporous structure, which is consistent with the nitrogen adsorption isotherm. The hydrogen storage densities of ACNF-1 and ACNF-2 at 77 K and 1 bar are 2.61 and 2.64 wt%, respectively. The atmospheric hydrogen storage density change is consistent with the change trend of specific surface area, total pore volume, ultramicroporous volume, and mesoporous volume, and it is not affected by the decrease in microporous volume. For the process of hydrogen desorption, the hydrogen desorption curve and the adsorption curve are approximately consistent within the pressure range of 1 bar to 0.45 bar. It is indicated that ACNF-1 and ACNF-2 have excellent reversible hydrogen storage performance, and hydrogen desorption can be completed only with the change in gas pressure alone, without the assistance of high temperature conditions. To evaluate the level of atmospheric hydrogen storage performance of the prepared activated carbon nanofibers, some gravimetric hydrogen storage densities at 77 K/1 bar are concluded for recently reported porous carbon hydrogen storage materials. As indicated in Table 3, ACNF-1 and ACNF-2 exhibit excellent atmospheric hydrogen storage performance (greater than 2.5 wt%), given that few porous carbon hydrogen storage materials have a gravimetric hydrogen storage density greater than 2.5 wt% at ambient pressure.

As shown in Fig. 5(b), the adsorption isotherm models are used to analyze the hydrogen adsorption process of activated carbon nanofibers. The Multisite-Langmuir ( $N = 3$ ) curve and Freundlich curve show the excellent fitting effect on the measured hydrogen adsorption data of ACNF-1 and ACNF-2 (Jung et al., 2009; Salvador et al., 2011; Bekeshov et al., 2023). For ACNF-1 and ACNF-2, the fitting variances  $R^2$  and Reduced Chi-Sqr of Multisite-Langmuir ( $N = 3$ ) model are better than that of Freundlich model (Table 2). It is indicated that the Multisite-Langmuir ( $N = 3$ ) model has a better fitting effect on the hydrogen adsorption isotherm of activated carbon nanofibers in the pressure range of 0-1 bar. In the Multisite-Langmuir ( $N = 3$ ) model of ACNF-1 and ACNF-2, the total saturated adsorption values of the three adsorption regions are

**Table 3.** Comparison with other reported porous carbon hydrogen storage materials.

Number	$S_{BET}$ (m <sup>2</sup> /g)	$V_{Tot}$ (cm <sup>3</sup> /g)	$V_{Micro}$ (cm <sup>3</sup> /g)	Hydrogen uptake at 1 bar, 77 K/wt%	Reference
CS-SE-AC	1,932	1.39	0.85	2.76	Park et al. (2020)
CS-SE	711	0.315	0.21	1.87	Park et al. (2020)
BG-S	1,703	2.12	0.51	1.53	Zhang et al. (2022)
TE-7	1,234	1.33	0.52	2.0	Ting et al. (2015)
TPC-1	1,940	1.23	0.36	2.02	Hu et al. (2014)
CCBC-1	1,688	2.17	0.53	1.8	Li et al. (2020)
CCBC-1.5	608	1.6	0.37	1.62	Li et al. (2020)
ACNF-1	1,994.03	0.94	0.83	2.61	This work
ACNF-2	2,007.66	1.01	0.78	2.64	This work

3.8441 and 3.9037, respectively. In addition, the Langmuir equilibrium constants  $K_{L1}$ ,  $K_{L2}$  and  $K_{L3}$  of ACNF-2 are 1.0272, 16.1459 and 336.5360 respectively.

#### 4. Conclusions

In this study, polyacrylonitrile-based ACNFs with high specific surface area of 2,007.66 m<sup>2</sup>/g were constructed based on electrospinning technology and ultrasonic-assisted activation technology for the application of atmospheric hydrogen storage. The nanopore structure of ACNFs was mainly composed of micropores, and the relative ratio of micropore volume and ultramicropore volume were 77.92% to 88.3% and 22.34% to 24.68% respectively. In addition, the surface groups of activated carbon nanofibers mainly included hydroxyl, carboxyl and pyridine. Attributed to the synergy of rich microporous structure and surface chemical structure, the atmospheric hydrogen storage density of ACNFs could reach 2.64 wt% at 77 K and 1 bar. After the optimization analysis of adsorption isotherm models, the Multisite-Langmuir ( $N = 3$ ) model was proved to be more suitable for accurate describing the atmospheric hydrogen adsorption process of ACNFs.

#### Acknowledgements

This work was supported by the National Natural Science Foundation of China (No. 51473088), the Natural Science Foundation of Shandong Province (No. ZR2022QE213), the Key Research and Development Plan of Shandong (No. 2018GGX102029) and the Open Fund of Guangdong Provincial Key Laboratory of Advanced Energy Storage Materials, South China University of Technology (No. 20212163).

#### Conflict of interest

The authors declare no competing interest.

**Open Access** This article is distributed under the terms and conditions of the Creative Commons Attribution (CC BY-NC-ND) license, which permits unrestricted use, distribution, and reproduction in any medium, provided the original work is properly cited.

#### References

- Ahn, D., Kim, D., Park, J. H., et al. Enhanced desalination performance of nitrogen-doped porous carbon electrode in redox-mediated deionization. *Desalination*, 2021, 520: 115333.
- Allendorf, M. D., Hulvey, Z., Gennett, T., et al. An assessment of strategies for the development of solid-state adsorbents for vehicular hydrogen storage. *Energy & Environmental Science*, 2018, 11: 2784-2812.
- Balahmar, N., Mokaya, R. Pre-mixed precursors for modulating the porosity of carbons for enhanced hydrogen storage: Towards predicting the activation behaviour of carbonaceous matter. *Journal of Materials Chemistry A*, 2019, 7(29): 17466-17479.
- Bekeshov, D., Ashimov, S., Wang, Y., et al. Understanding gas-enhanced methane recovery in graphene nanoslits via molecular simulations. *Capillarity*, 2023, 6(1): 1-12.
- Blankenship, I. T. S., Balahmar, N., Mokaya, R. Oxygen-rich microporous carbons with exceptional hydrogen storage capacity. *Nature Communications*, 2017, 8(1): 1545.
- Chen, Z., Li, P., Anderson, R., et al. Balancing volumetric and gravimetric uptake in highly porous materials for clean energy. *Science*, 2020, 368(6488): 297-303.
- Díez, N., Mysyk, R., Zhang, W., et al. One-pot synthesis of highly activated carbons from melamine and terephthalaldehyde as electrodes for high energy aqueous supercapacitors. *Journal of Materials Chemistry A*, 2017, 5(28): 14619-14629.
- Fan, Z., Yan, J., Wei, T., et al. Asymmetric supercapacitors based on graphene/MnO<sub>2</sub> and activated carbon nanofiber electrodes with high power and energy density. *Advanced Functional Materials*, 2011, 21(12): 2366-2375.
- Haddad, M. Y., Alharbi, H. F. Enhancement of heavy metal ion adsorption using electrospun polyacrylonitrile nanofibers loaded with ZnO nanoparticles. *Journal of Applied Polymer Science*, 2018, 136(11): 47209.
- Hu, X., Chen, Q., Zhao, Y., et al. Straightforward synthesis of a triazine-based porous carbon with high gas-uptake capacities. *Journal of Materials Chemistry A*, 2014, 2(34):

- 14201-14208.
- Ismar, E., Sarac, A. S. Oxidation of polyacrylonitrile nanofiber webs as a precursor for carbon nanofiber: aligned and non-aligned nanofibers. *Polymer Bulletin*, 2017, 75(2): 485-499.
- Jaramillo, D. E., Jiang, H., Evans, H. A., et al. Ambient-temperature hydrogen storage via Vanadium(II)-dihydrogen complexation in a metal-organic framework. *Journal of the American Chemical Society*, 2021, 143(16): 6248-6256.
- Jung, M. J., Kim, J. W., Im, J. S., et al. Nitrogen and hydrogen adsorption of activated carbon fibers modified by fluorination. *Journal of Industrial and Engineering Chemistry*, 2009, 15(3): 410-414.
- Kim, H., Lee, D., Moon, J. Co-electrospun Pd-coated porous carbon nanofibers for hydrogen storage applications. *International Journal of Hydrogen Energy*, 2011, 36(5): 3566-3573.
- Kizildag, N., Ucar, N., Onen, A., et al. Polyacrylonitrile/polyaniline composite nanofiber webs with electrostatic discharge properties. *Journal of Composite Materials*, 2016, 50(28): 3981-3994.
- Li, Y., Teliz, E., Zinola, F., et al. Design of a AB5-metal hydride cylindrical tank for hydrogen storage. *International Journal of Hydrogen Energy*, 2021, 46(68): 33889-33898.
- Li, X., Zhang, H., Zhao, B., et al. Preparation of hydrogen storage carbon materials using bio-oil heavy components as carbon-containing precursor. *Fuel Processing Technology*, 2020, 203: 106386.
- Lim, D. W., Yoon, J. W., Ryu, K. Y., et al. Magnesium nanocrystals embedded in a metal-organic framework: hybrid hydrogen storage with synergistic effect on physical and chemisorption. *Angewandte Chemie International Edition*, 2012, 51(39): 9814-9817.
- Liu, J., Chen, G., Gao, H., et al. Structure and thermochemical properties of continuous bundles of aligned and stretched electrospun polyacrylonitrile precursor nanofibers collected in a flowing water bath. *Carbon*, 2012, 50(3): 1262-1270.
- Liu, J., Zhang, T., Sun, S. Stability analysis of the water bridge in organic shale nanopores: A molecular dynamic study. *Capillarity*, 2022, 5(4): 75-82.
- Madrakian, T., Mohammadzadeh, A. H., Maleki, S., et al. Preparation of polyacrylonitrile nanofibers decorated by N-doped carbon quantum dots: Application as a fluorescence probe for determination of Cr(VI). *New Journal of Chemistry*, 2018, 42(23): 18765-18772.
- Mahdi, D. S., Al-Khdheewi, E. A., Yuan, Y., et al. Hydrogen underground storage efficiency in a heterogeneous sandstone reservoir. *Advances in Geo-Energy Research*, 2021, 5(4): 437-443.
- Nguyen, D. H., Kim, J. H., Vo, T. T. N., et al. Design of portable hydrogen tank using adsorption material as storage media: An alternative to type IV compressed tank. *Applied Energy*, 2022, 310: 118552.
- Park, J. H., Park, S. J. Expansion of effective pore size on hydrogen physisorption of porous carbons at low temperatures with high pressures. *Carbon*, 2020, 158: 364-371.
- Qiao, K., Yu, J., Zhu, B., et al. Oxygen-rich activated carbon fibers with exceptional Cu(II) adsorptivity and recycling performance. *Industrial & Engineering Chemistry Research*, 2020, 59(29): 13088-13094.
- Real, C. G., Vicentini, R., Nunes, W. G., et al. Analyses of dispersive effects and the distributed capacitance in the time and frequency domains of activated carbon nanofiber electrodes as symmetric supercapacitors. *Electrochimica Acta*, 2022, 402: 139299.
- Sahoo, S. K., Panigrahi, G. K., Sahoo, J. K., et al. Electrospun magnetic polyacrylonitrile-GO hybrid nanofibers for removing Cr(VI) from water. *Journal of Molecular Liquids*, 2021, 326: 115364.
- Salvador, F., Montero, J., Sánchez-Montero, M. J., et al. Mechanism of heterogeneous adsorption in the storage of hydrogen in carbon fibers activated with supercritical water and steam. *International Journal of Hydrogen Energy*, 2011, 36(13): 7567-7579.
- Schoedel, A., Ji, Z., Yaghi, O. M. The role of metal-organic frameworks in a carbon-neutral energy cycle. *Nature Energy*, 2016, 1(4): 16034.
- Smith, J. W. H., McDonald, M., Romero, J. V., et al. Small and wide angle X-ray studies of impregnated activated carbons. *Carbon*, 2014, 75: 420-431.
- Sun, Q., Wang, N., Xu, Q., et al. Nanopore-supported metal nanocatalysts for efficient hydrogen generation from liquid-phase chemical hydrogen storage materials. *Advanced Materials*, 2020, 32(44): 2001818.
- Tan, N. P. B., Dadol, G. C., Cabatingan, L. K., et al. Solution blow spinning (SBS)-polyacrylonitrile (PAN)-assisted cellulose acetate nanofiber membrane. *Nanotechnology*, 2020, 31(34): 345602.
- Ting, V. P., Ramirez-Cuesta, A. J., Bimbo, N., et al. Direct evidence for solid-like hydrogen in a nanoporous carbon hydrogen storage material at supercritical temperatures. *ACS Nano*, 2015, 9(8): 8249-8254.
- Waisi, B. I., Manickam, S. S., Benes, N. E., et al. Activated carbon nanofiber nonwovens: improving strength and surface area by tuning fabrication procedure. *Industrial & Engineering Chemistry Research*, 2019, 58(10): 4084-4089.
- Wang, S., Chen, L., Feng, Q., et al. Pore-scale simulation of gas displacement after water flooding using three-phase lattice Boltzmann method. *Capillarity*, 2023, 6(2): 19-30.
- Wang, Y., Chen, X., Zhang, H., et al. Heterostructures built in metal hydrides for advanced hydrogen storage reversibility. *Advanced Materials*, 2020, 32(31): 2002647.
- Wu, R., Zhang, X., Liu, Y., et al. A unique double-layered carbon nanobowl-confined lithium borohydride for highly reversible hydrogen storage. *Small*, 2020, 16(32): 2001963.
- Xu, Y., Zhang, C., Zhou, M., et al. Highly nitrogen doped carbon nanofibers with superior rate capability and cyclability for potassium ion batteries. *Nature Communication*, 2018, 9(1): 1720.
- Ying, Z., Shao, Z., Wang, L., et al. Sol-Gel SiO<sub>2</sub> on electrospun polyacrylonitrile nanofiber for efficient oil-in-water

- emulsion separation. *Journal of Materials Science*, 2020, 55(34): 16129-16142.
- Yu, J., Chen, F., Yan, S., et al. Facile fabrication of N/O co-doped activated carbon hollow fibers for hydrogen storage at atmospheric pressure. *Polymer Bulletin*, 2023, 80(2): 1385-1397.
- Yu, J., Meng, Z., Yan, S., et al. Precise control of ultramicropore structure of activated carbon fiber for the application of Cu(II) adsorption/electro-adsorption. *Journal of Environmental Chemical Engineering*, 2021, 9(4): 105312.
- Yuan, W., Ge, M., Wang, K., et al. Atomic-scale selectivity of hydrogen for storage sites in Pd nanoparticles at atmospheric pressure. *Nanoscale*, 2019, 11(21): 10198-10202.
- Zakaria, A. F., Kamaruzaman, S., Rahman, N. A. Electrospun polyacrylonitrile/ lignin/poly(ethylene glycol)-based porous activated carbon nanofiber for removal of Nickel(II) ion from aqueous solution. *Polymers*, 2021, 13(20): 3590.
- Zhang, Y., Zhu, B., Cai, X., et al. Rapid in situ polymerization of polyacrylonitrile/graphene oxide nanocomposites as precursors for high-strength carbon nanofibers. *ACS Applied Materials & Interfaces*, 2021, 13(14): 16846-16858.
- Zhang, H., Zhu, Y., Liu, Q., et al. Preparation of porous carbon materials from biomass pyrolysis vapors for hydrogen storage. *Applied Energy*, 2022, 306: 118131.